COMMUNICATION

An octacoordinated Nb atom in the $NbAl_8H_8^+$ cluster

Piero Ferrari,[a] Hung Tan Pham,[b] Jan Vanbuel,[a] Minh Tho Nguyen,[c,*] André Fielicke[d] and Ewald Janssens[a,*]

Received 00th January 20xx,
Accepted 00th January 20xx

DOI: 10.1039/x0xx00000x

The $NbAl_8H_8^+$ cluster was formed in a molecular beam and characterized by mass spectrometry and infrared spectroscopy. Density functional theory calculations show the lowest-energy isomer is a high symmetry singlet with the Nb atom placed at the center of a distorted hexagonal Al ring and coordinated by two AlH moieties, therefore exhibiting octacoordination. The unprecedented high-symmetric geometry is attributed to the 20 valence electrons; the central Nb atom adheres to the 18-electron rule and two additional delocalized electrons stabilize the hexagonal ring.

Coordination chemistry is a rich and vibrant field of research, featuring applications ranging from catalysis and medicine to optics and magnetism. Examples of novel forms of coordination include a monocyclic boron wheel [1, 2] and anticipated but yet unobserved planar pentacoordinate carbon species [3]. Also in more classical Wernerian coordination chemistry, recent examples of exotic coordination can be found in literature, such as eight-coordinate carbonyl and dinitrogen complexes of calcium, strontium, and barium in a solid neon matrix [4, 5].

Many stable compounds with unprecedented coordination can be understood by the electron counting rules introduced by Langmuir [6]. Those rules for delocalized valence electrons around a central atom prescribe a more stable complex for closed-electronic configurations with 8, 18, 20 or 32 itinerant electrons [7]. While the octet rule explains the stability of compounds like methane and water, the 18-electron rule is commonly used to rationalize the stability of transition metal complexes, such as the metal carbonyl compounds $Ni(CO)_4$, $Fe(CO)_5$, and $Mo(CO)_6$ [8]. This rule also has been used to explain the stability of all-metal clusters like WAu_{12} [9] and the formation of stable eight-coordinated $M(CO)_8$ (M = Ca, Sr, or Ba) [10]. The stability of the $Th(C_8H_8)_2$ complex, instead, is explained by a 20-electron counting [7].

For the Nb atom, the reported maximal number of homoleptic, monodentate ligands is seven [11, 12], although bidentate eightfold-coordinated peroxo-complexes have been observed before [13]. Larger Nb coordination numbers exist for non-classical complexes like the planar $Nb@B_{10}^-$ boron wheel, which has been identified via a combination of photoelectron spectroscopy and density functional theory (DFT) calculations [14]. Besides being of fundamental interest, niobium and its oxides are used as catalytic promotors and support a variety of industrial reactions like alcohol dehydration, NO reduction, and Fischer esterification [15, 16]. As catalysis is often limited to a few active sites, in the past decade the new research branch of single or few-atom catalysts developed [17, 18, 19]. Ahn *et al*., for example, showed that niobium can be used to decorate a metal-organic-framework and catalyse alkene epoxidation [20]. Zhang *et al*. incorporated single Nb atoms in graphene layers, enabling the catalytic reduction of oxygen [21]. The Böhme group have found that Nb^+ is the lightest transition metal ion that inserts into methane C-H bonds via H_2 elimination [22]. Catalytic hydrogenation has been observed for niobium doped sodium alanate [23]. Sodium alanate contains a high weight percentage of hydrogen and is attractive for hydrogen storage applications [24].

In this context, we set out to investigate the hydrogen binding geometry of hydrogenated Nb doped Al clusters, by combining infrared multiple photon dissociation (IRMPD) spectroscopy with DFT calculations. We identified $NbAl_8H_8^+$ as a highly symmetric, non-classic coordination complex with a central Nb atom coordinated by a distorted hexagonal Al ring and two AlH ligands. Analysis of its electronic structure revealed that the complex is stabilized by 20 valence electrons.

$NbAl_n^+$ ($n \leq 12$) clusters were produced in a dual-laser (Nd:YAG third harmonic, 15 mJ per pulse) vaporization source [25], using He as carrier gas. The hydrogenated complexes were formed by adding H_2 gas via a pulsed valve connected directly to the source nozzle, which is kept at room temperature. After production, the clusters were analysed by an orthogonal time-of-flight mass spectrometer. To probe the hydrogen binding geometry of the clusters, IRMPD experiments were performed at the free electron laser (FEL) facility of the Fritz Haber Institute [26]. The FEL was optimized to provide an intense (~50 mJ per

[a] Quantum Solid-State Physics, KU Leuven, Celestijnenlaan 200D, 3001 Leuven, Belgium. Email: ewald.janssens@kuleuven.be
[b] Department of Chemistry, KU Leuven, Celestijnenlaan 200F, 3001 Leuven, Belgium.
[c] Institute for Computational Science and Technology (ICST), Ho Chi Minh City, Vietnam. Email: tho.nm@icst.org.vn
[d] Fritz-Haber-Institut der Max-Planck-Gesellschaft, Faradayweg 4–6, 14195 Berlin, Germany.
Electronic Supplementary Information (ESI) available. See DOI: 10.1039/x0xx00000x

pulse) photon beam in the 800–2050 cm^{-1} spectral range, which is the characteristic region of the vibrational modes of metal-hydrogen and metal-dihydrogen bonds [27, 28]. Following resonant absorption of infrared photons, the excited $NbAl_nH_{2p}^+$ clusters fragment by the loss of hydrogen molecules, as detected mass spectrometrically [29]. Mass spectra with and without FEL interaction were recorded alternatingly to minimize the effect of fluctuations in the cluster signal intensity on the depletion spectra. The experimental yield is defined as $\sigma_{exp}(\nu) = \log(I_0/I_{FEL})/P(\nu)$, where I_0/I_{FEL} is the abundance ratio of the cluster without and with the FEL crossing the molecular beam and $P(\nu)$ the laser pulse energy.

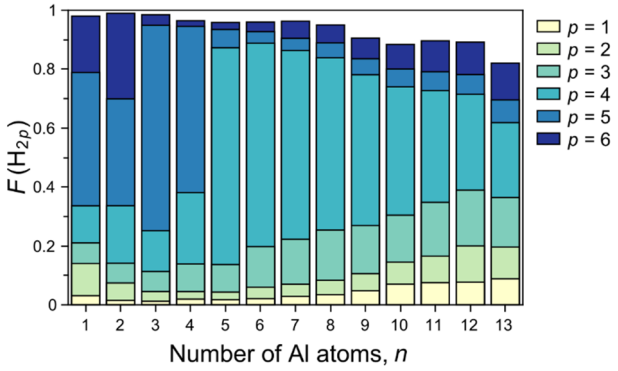

Figure 1. Fractional distribution of hydrogen in $NbAl_nH_{2p}^+$ clusters (n = 1 – 13, p = 0 – 6).

Figure 1 presents the fractional distribution of $NbAl_nH_{2p}^+$ (p = 0 – 6) clusters. A representative mass spectrum is presented in the supporting information (SI). The distribution is defined as $F(H_{2p}) = I(NbAl_nH_{2p}^+)/\sum_i I(NbAl_nH_{2i}^+)$, with I the abundance of the cluster within brackets in the mass spectrum. Up to n = 4, mostly five H_2 molecules are adsorbed per cluster, while for all larger sizes, $n \geq 5$, the largest fraction is that of four H_2 molecules. In the entire size range investigated, up to six H_2 can be adsorbed per cluster. This large amount of hydrogen adsorbed on these clusters stands in stark contrast to the results of previous studies under similar conditions on V and Rh doped Al clusters, for which only one or two H_2 molecules were found to adsorb for $n > 4$ [27, 29, 30]. Moreover, pure Al_n^+ clusters, with the exception of $Al_{6,7}^+$ [27, 31], are known to be unreactive towards H_2. This observation hints that aluminium-based nanostructures, such as aluminium nanoparticles or aluminium porous materials, containing traces of niobium, might be useful for hydrogen storage purposes. The distribution in Figure 1 is even more puzzling in view of work on the reaction between molecular hydrogen and small pure Nb clusters, in which no hydrogenated species were seen [32, 33, 34, 35].

Representative IRMPD spectra for $NbAl_5H_8^+$, $NbAl_6H_8^+$, and $NbAl_8H_8^+$ clusters are shown in Figure 2. Spectra of other sizes are available in the SI. Three distinctive features can be discerned in the experimental spectra: only $NbAl_2H_{12}^+$ has a band in the low wavenumber regime (around 850 cm^{-1}, see SI); several bands locate between 1000 cm^{-1} and 1600 cm^{-1} (strong for $NbAl_5H_8^+$); and an intense band around 1900 cm^{-1} is seen for all sizes. In pure metallic clusters, vibrational modes tend to involve a convoluted displacement of the atoms. Given the mass difference between hydrogen and Nb or Al, the vibrations above 800 cm^{-1} mostly involve large H displacements. Characteristic wavelengths of different vibrational modes were identified in previous studies on transition metal doped aluminium clusters [29, 27, 30], and for the current clusters confirmed by the DFT calculations. The band around 850 cm^{-1} corresponds to a metal-H_2 stretch mode for molecularly adsorbed hydrogen. The bands in the 1000–1600 cm^{-1} range originate from μ_2 bridge Al-H-Al and Al-H-Nb vibrations, or μ_3 coordinated hydrogen. Niobium hydride bands are expected between 1600–1850 cm^{-1} [36], while the bands above 1900 cm^{-1} correspond to stretching vibrations of Al on-top-bound H atoms. Examples of selected vibrational modes of $NbAl_8H_{2p}^+$ clusters are visualised in the SI.

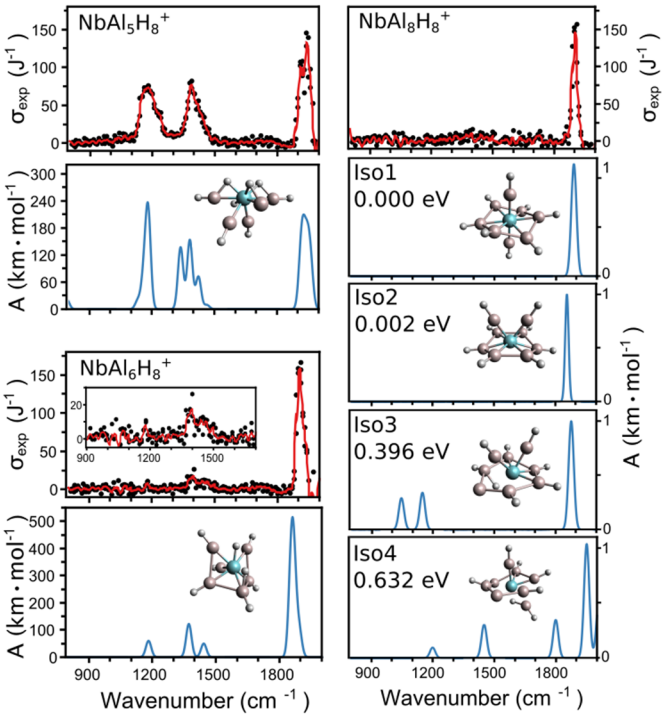

Figure 2. IRMPD spectra of $NbAl_nH_8^+$ (n = 5, 6, 8). Raw data is shown in black, with a three-point moving average in red. For n = 6, the inset contains a zoom of the 900–1700 cm^{-1} region. Below the n = 5 and 6 experimental spectra, calculated IR spectra of the putative ground state isomer are presented. For n = 8, calculated spectra of the four lowest-energy isomers are shown.

Remarkably, for clusters with $n \geq 8$, the band at 1900 cm^{-1} is the only feature in the IRMPD spectra. This implies that either 1) all H atoms are bound on-top the Al atoms, or 2) if some H atoms take other positions their corresponding vibrations are not infrared active. That conjecture agrees with the calculations predicting exclusive dissociated hydrogen on-top of Al atoms for $n \geq 8$ (see further).

The measured IRMPD spectra are compared with vibrational spectra computed by DFT calculations. Low energy isomers of $NbAl_nH_m^+$ ($n \leq 9$) clusters were searched by a stochastic genetic algorithm generating probable initial structures [37]. For this purpose, the algorithm by Saunders [38] was modified by a module that checks all the generated isomers and eliminates unphysical structures, before a geometric optimization with the Gaussian 09 package [39]. All initial geometries were optimized

using the hybrid TPSSh functional and the small LANL2DZ basis set. The lower-lying structures were subsequently characterized by harmonic vibrational frequencies, before scrutinizing them further by employing the TPSSh functional and the larger aug-cc-pVTZ basis set for Al, H, and aug-cc-pVTZ-PP for Nb. The selection of this theory level is motivated in the SI. As shown in Figure 2, the frequencies and even relative intensities of the computed infrared spectra of the lowest energy isomers of $NbAl_5H_8^+$ and $NbAl_6H_8^+$ agree well with the experiment (no scaling factor applied). For both clusters, the bands between 1100 and 1500 cm^{-1} are reproduced by the calculations, in addition to the intense modes around 1900 cm^{-1}.

The infrared spectrum of $NbAl_8H_8^+$ is shown in the top-right panel of Figure 2. For this species only a band at 1895 cm^{-1}, characteristic for Al-H stretches, is found. Infrared spectra of four lowest-energy isomers are compared to the experiment. The geometry of the lowest-energy isomer Iso1 has a high symmetry (D_{3d}), i.e. a distorted hexagon around a central Nb atom, coordinated by two AlH moieties. The remarkable geometry of Iso1, with an octacoordinated central Nb atom, is presented more clearly in Figure 3a. The symmetry of this isomer is reflected in its calculated infrared spectrum, which contains only two, almost degenerate, modes of e_u symmetry around 1880 cm^{-1} in perfect agreement with experiment. Both Iso3 and Iso4 are significantly higher in energy and have one H atom in μ_3 and μ_2 coordinations, respectively; therefore, these isomers have modes between 1000 and 1600 cm^{-1}. The calculated infrared spectrum of Iso2, only 0.002 eV higher in energy than Iso1 and also having exclusively H atoms atop the Al atoms, agrees as well with the experiment. Hence, Iso1 and Iso2 cannot be distinguished by the experimental data. Nevertheless, in both isomers the H atoms adopt solely atop Al positions, instead of binding with the reactive Nb dopant, and both have an octacoordinated Nb atom. The main difference is in the position of the two AlH moieties, on the same and opposite sides of the Al_6H_6 ring for Iso1 and Iso2, respectively.

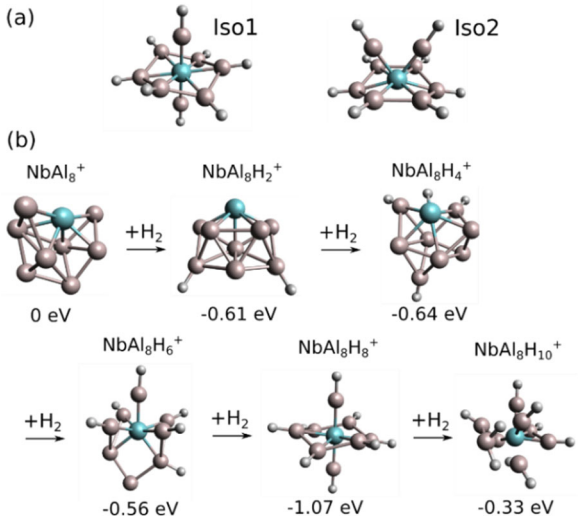

Figure 3. (a) Geometry of the two lowest-energy isomers of $NbAl_8H_8^+$. (b) Hydrogenation steps from $NbAl_8^+$ to $NbAl_8H_{10}^+$. Upon hydrogenation, the cluster adopts a more open structure, with AlH moieties ligating the central Nb ion in $NbAl_8H_8^+$. The (free) energy stabilization (at 300 K) of each hydrogenation step, calculated at theTPSSh/aug-cc-pVTZ-PP level, is also listed.

A remarkable feature of the $NbAl_8^+$ cluster is that it completely rearranges following H_2 adsorption and dissociation (which occurs spontaneously). This is highlighted in Figure 3b, presenting the calculated formation path of $NbAl_8H_8^+$ (Iso1) via successive adsorption of H_2 molecules. $NbAl_8^+$ is a compact metal cluster with an eccentric Nb atom. The hydrogenation path consists of sequential adsorption of H_2 on top of the Nb atom. H_2 then dissociates and spills over the Al atoms. Each H_2 adsorption is exothermic, with the largest energy gain for the fourth H_2 molecule (1.07 eV) to reach the symmetric $NbAl_8H_8^+$. Further stabilization occurs when adding a fifth H_2 molecule, but the energy gain is smaller than in the previous steps.

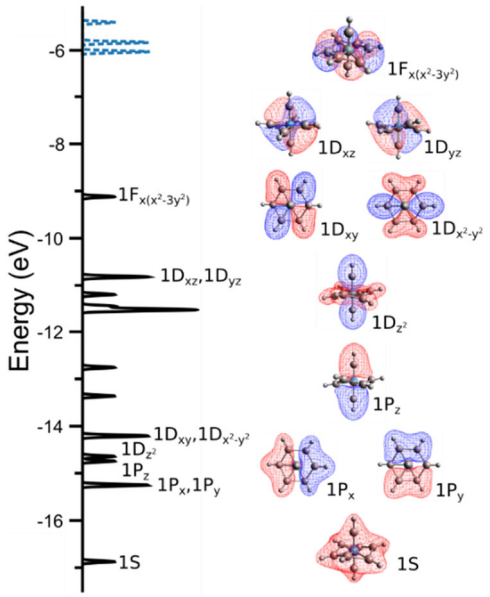

Figure 4. Density of states of the $NbAl_8H_8^+$ (Iso1) cluster. Occupied (empty) states are represented in black (blue). Molecular orbitals of delocalized character are shown in the right side of the figure, with a label of their corresponding symmetry (TPSSh/aug-cc-pVTZ-PP).

To explore the chemical bonding in $NbAl_8H_8^+$, the electron density of Iso1 is examined. An analysis using the electron localization function (ELF, presented in the SI), reveals that the six AlH groups in the Al hexagon connect through Al-Al bonds, resulting in a $(AlH)_6$ cycle and that the electrostatic interaction is important in the bonding between Nb and the $(AlH)_6$ hexagon. This agrees with the Löwdin net charges of the cluster, with the Nb atom having a negative charge of -1.3 e, whereas the charge of each AlH unit in the $(AlH)_6$ cycle is +0.2 e. The remaining two AlH groups, on top and below the $(AlH)_6$ cycle, form a delocalized bonding along the AlH-Nb-AlH axis to the $Nb@(AlH)_6$ hexagonal cycle. These AlH groups also donate electrons to $Nb@(AlH)_6$, as their net charge is +0.5 e each.

A map of density of states of Iso1 is depicted in Figure 4. The occupied (empty) states are shown in back (blue). The MOs are shown in the right side of Figure 4 and labelled based on their nodal character. The HOMO-LUMO gap of the cluster is

considerably large, close to 3.1 eV. Of the occupied MOs of the cluster, ten possess a delocalized wavefunction resembling an electronic configuration of $\{1S^2|1P^6|1D^{10}|1F_{x(x^2-3y^2)}{}^2\}$. Since these MOs are doubly occupied in the singlet ground state, the $NbAl_8H_8^+$ cluster has in total 20 delocalized valence electrons. The filled $1S^2|1P^6|1D^{10}$ orbitals around the central Nb atom adhere with the 18-electron rule, while the $1F_{x(x^2-3y^2)}$ orbital delocalizes on the $Nb@(AlH)_6$ hexagonal cycle, stabilizing it. A similar electron-counting rule applies for Iso2 of $NbAl_8H_8^+$, with a considerably large HOMO-LUMO gap of 2.8 eV. The density of states analysis of Iso2 is available in the SI.

In summary, by combining experimental and computational studies, we have shown the formation of the niobium-doped aluminum $NbAl_8H_8^+$ cluster and demonstrated its non-classical geometric and electronic features. In its high symmetry singlet ground state, the Nb dopant is placed at the centre of a distorted hexagon, with two coordinated AlH groups, therefore exhibiting a coordination number of eight.

Acknowledgements.

The authors thank Gerard Meijer for his continuing support. This work is supported by the KU Leuven Research Council (C14/18/073) and the Research Foundation Flanders (FWO, G.0A05.19N). P.F. and J.V. thank the FWO and A.F. the Deutsche Forschungsgemeinschaft for a Heisenberg grant (FI893/5). The work of M. T. N. and H. T. P. was founded by VinGroup (Vietnam) and supported by VinGroup Innovation Foundation (VinIF) under project code VINIF.2020.DA21. Resources and services used in this work were provided by the VSC (Flemish Supercomputer Center), funded by the FWO and the Flemish Government. Part of the work has been performed under the Project HPC-EUROPA3 (INFRAIA-2016-1-730897), with the support of the European Commission H2020 Programme. P.F. acknowledges support of the Department of Inorganic and Organic Chemistry of the University of Barcelona, and computer resources and technical support provided by the Barcelona Supercomputer Centre.

Notes and references

1 I. A. Popov, T. Jian, G. V. Lopez, A. I. Boldyrev and L.-S. Wang, *Nat. Comm.* 2015, **6**, 8654.
2 C. Romanescu, T. R. Galeev, W.-L. Li, A. I. Boldyrev and L.-S. Wang, *Acc. Chem. Res.*, 2013, **46**, 350.
3 V. Vassilev-Galindo, S. Pan, K. J. Donald and G. Merino, *Nat. Rev. Chem.,* 2018, **2**, 0114.
4 X. Wu, L. Zhao, J. Jin, S. Pan, W. Li, X. Jin, G. Wang, M. Zhou and G. Frenking, *Science*, 2018, **361**, 912.
5 Q. Wang, S. Pan, S. Lei, J. Jin, G. Deng, G. Wang, L. Zhao and M. F. G. Zhou, *Nat. Commun.*, 2019, **10**, 3375.
6 I. Langmuir, *Science*, 1921, **54**, 59.
7 P. Pyykkö, *J. Organomet. Chem.*, 2006, **691**, 4336.
8 S. C. Rasmussen, *ChemTexts*, 2015, **1**, 10.
9 P. Pyykkö and N. Runeberg, *Angew. Chem. Int. Ed.*, 2002, **41**, 2174.
10 P. B. Armentrout, *Science*, 2018, **361**, 849.
11 A. M. Ricks, Z. D. Reed and M. A. Duncan, *J. Am. Chem. Soc.*, 2009, **131**, 9176.
12 A. M. Ricks, Z. E. Reed and M. A. Duncan, *J. Mol. Spectrosc.*, 2011, **266**, 63.
13 D. Bayot, M. Devillers and D. Peeters, *Eur. J. Inorg. Chem.*, 2005, **2005**, 4118.
14 T. R. Galeev, C. Romanescu, W. L. Li, L. S. Wang and A. I. Boldyrev, *Angew. Chem. Int. Ed.*, 2012, **51**, 2101.
15 I. Nowak and M. Ziolek, *Chem. Rev.*, 1999, **99**, 3603.
16 K. Tanabe, *Catal. Today*, 2003, **78**, 65.
17 D. K. Bohme and H. Schwarz, *Angew. Chem. Int. Ed.*, 2005, **44**, 2336.
18 X. F. Yang, A. Wang, B. Qiao, J. Li, J. Liu and T. Zhang, *Acc. Chem. Res.*, 2013, **46**, 1740.
19 E. C. Tyo and S. Vajda, *Nat. Nanotechnol.*, 2015, **10**, 577.
20 S. Ahn, N. E. Thornburg, Z. Li, T. C. Wang, L. C. Gallington, K. W. Chapman, J. M. Notestein, J. T. Hupp and O. K. Farha, *Inorg. Chem.*, 2016, **55**, 11954.
21 X. Zhang, J. Guo, P. Guan, C. Liu, H. Huang, F. Xue, X. Dong, S. J. Pennycook and M. F. Chisholm, *Nat. Commun.*, 2013, **4**, 1924.
22 A. Shayesteh, V. V. Lavrov, G. K. Koyanagi and D. K. Bohme, J. *Phys. Chem. A*, 2009, **113**, 5602.
23 J. Mao, Z. Guo and H. Liu, *Int. J. Hydrog. Energy*, 2011, **36**, 14503.
24 M. B. Ley, L. H. Jepsen, Y. S. Lee, Y. W. Cho, J. M. Von Colbe, M. Dornheim, M. Rokni, J. O. Jensen, M. Sloth, Y. Filinchuk and J. E. Jørgensen, *Mater. Today*, 2014, **17**, 122.
25 N. X. Truong, B. K. A. Jaeger, S. Gewinner, W. Schöllkopf, A. Fielicke and O. Dopfer, *J. Phys. Chem. C*, 2017, **121**, 9560.
26 W. Schöllkopf, S. Gewinner, H. Junkes, A. Paarmann, G. von Helden, H. Bluem and A. M. M. Todd, *Proc. SPIE*, 2015, **9512**, 95121L.
27 J. Vanbuel, M.-y. Jia, P. Ferrari, S. Gewinner, W. Schöllkopf, M. T. Nguyen, A. Fielicke and E. Janssens, *Top. Catal.*, 2018, **61**, 62.
28 I. Swart, F. M. F. de Groot, B. M. Weckhuysen, P. Gruene, G. Meijer and A. Fielicke, *J. Phys. Chem. A*, 2008, **112**, 1139.
29 J. Vanbuel, E. M. Fernández, P. Ferrari, S. Gewinner, W. Schöllkopf, L. C. Balbás, A. Fielicke and E. Janssens, *Chem. Eur. J.*, 2017, **23**, 15638.
30 M. Jia, J. Vanbuel, P. Ferrari, E. M. Fernández, S. Gewinner, W. Schöllkopf, M. T. Nguyen, A. Fielicke and E. Janssens, *J. Phys. Chem. C*, 2018, **122**, 18247.
31 I. Pino, G. J. Kroes and M. C. Van Hemert, *J. Chem. Phys.*, 2010, **133**, 184304.
32 C. Berg, T. Schindler, G. Niedner-Schatteburg and V. E. Bondybey, *J. Chem. Phys.*, 1995, **102**, 4870.
33 J. L. Elkind, F. D. Weiss, J. M. Alford, R. T. Laaksonen and R. E. Smalley, *J. Chem. Phys.*, 1988, **88**, 5215.
34 M. E. Geusic, M. D. Morse and R. E. Smalley, *J. Chem. Phys.*, 1985, **82**, 590.
35 A. B. Vakhtin and K. Sugawara, *J. Chem. Phys.*, 1999, **111**, 10859.
36 X. Wang and L. Andrews, *J. Phys. Chem. A*, 2011, **115**, 14175.
37 H. P. Pham, L. V. Duong, B. C. Pham and M. T. Nguyen, *Chem. Phys. Lett.*, 2013, *577*, 32.
38 M. Saunders, *J. Comput. Chem.*, 2004, **25**, 621.
39 M. J. Frisch, G. W. Trucks, H. B. Schlegel, G. E. Scuseria, M. A. Robb et al., Gaussian, Inc., Wallingford CT, 2016.

